

# Rectifying Nanoscale Electron Transfer by Viologen Moieties and Hydrophobic Electrolyte Ions<sup>†</sup>

Shaowei Chen\* and Fengjun Deng

Department of Chemistry, Southern Illinois University, Carbondale, Illinois 62901

Received May 19, 2002. In Final Form: August 14, 2002

The rectifying effects of electrolyte ions on interfacial electron transfers were investigated with a gold nanoparticle monolayer anchored by bifunctional chemical bridges with viologen moieties. Gold nanoparticle monolayers were fabricated by using a sequential anchoring mechanism with viologen dithiols as the chemical linkers. For viologen monolayers, the voltammetric currents were found to be sensitive to electrolyte ions. Due to the ion-pair formation between the bipyridinium moieties and hydrophobic anions, the electron-transfer kinetics of the viologen functional groups seems impeded by the increasing concentration of “soft” ions, leading to the diminishment of the faradaic currents. This response to electrolyte ions is in great contrast to that of gold nanoparticle monolayers, where the quantized charging currents become better-defined with increasing concentration of hydrophobic ions. By hybridizing these conventional and nanoscale redox-active entities into the interfacial organized structure, one can manipulate interfacial charge transfer, where the voltammetric responses behave analogously to Coulomb blockade with the currents rectified at either negative or positive electrode potentials, depending on the nature of the electrolyte ions.

## Introduction

Alkanethiolate-protected gold nanoparticles exhibit quantized charging to their molecular capacitance in solutions, i.e., the so-called electrochemical analogue to the conventional Coulomb staircase,<sup>1</sup> and these discrete charge-transfer processes can be rectified by simple hydrophobic electrolyte ions in aqueous solutions with nanoparticle surface organized monolayers.<sup>2</sup> These single-electron-transfer characters demonstrate the application potentialities of using these nanoscale entities as the building blocks for the fabrication of novel electronic devices/circuits. To this end, effective methods for constructing nanoparticle organized assemblies must be developed and their charge-transfer chemistry has to be probed. Thus far, a wide variety of effective routes<sup>3,4</sup> have been developed to construct surface ordered ensembles of gold nanoparticles, and the general principle lies in using

bifunctional linkers where one end anchors to the substrate surface while the other end does so to the particle molecules. In these chemical bridges, redox-active moieties can be incorporated to investigate the effects of their electronic structure on the charge-transfer chemistry involved in the surface nanoensembles. For instance, Schiffrin and co-workers<sup>4d</sup> utilized viologen dithiols to generate multilayer structures of “naked” gold nanoparticles (diam 6 nm) by a layer-by-layer adsorption route. They found that within a certain thickness of the surface layers, the viologen moieties were electrochemically addressable and exhibited electron-mediating properties for an external redox couple,  $[\text{Ru}(\text{NH}_3)_6]^{3+/2+}$ . In addition, when viologen dithiols were present in the outer layer, the electroreduction of the ruthenium complex was facilitated, whereas the reverse oxidation process was hindered, leading to a voltammetric response similar to that of a molecular diode.<sup>4d</sup> In this study, the sole purpose of the presence of gold nanoparticles seems only to serve as the supporting matrix for the viologen multilayer structure. The electron-transfer properties associated with the nanosized particle molecules were not probed.

The discrete charging characters observed previously with nanosized gold particles represent a novel electrochemical charge-transfer phenomenon. It is understood in the context of successive  $1e^-$  charging to the (sub)-attofarad molecular capacitance of the nanoparticle molecules.<sup>1</sup> More importantly, in aqueous solutions containing hydrophobic electrolyte anions, well-defined quantized charging to nanoparticle surface assemblies can be initiated but only at potentials more positive than the particle potential of zero charge (PZC), whereas in the negative potential regime, the current is significantly smaller.<sup>2</sup> This rectifying behavior is ascribed to the capacitive nature of these electron-transfer processes on the basis of a Randle's equivalent circuit, where the ion-pair formation between hydrophobic ions and nanoparticle molecules leads to variation of the electrode interfacial capacitance.<sup>2</sup> In addition, by manipulating the electrolyte composition, one can observe a transition where the voltammetric responses evolve from those of a

<sup>†</sup> Dedicated to Dr. James W. Neckers on the occasion of his 100<sup>th</sup> birthday.

\* To whom all correspondence should be addressed. E-mail: schen@chem.siu.edu.

(1) (a) Ingram, R. S.; Hostetler, M. J.; Murray, R. W.; Schaaff, T. G.; Khoury, J.; Whetten, R. L.; Bigioni, T. P.; Guthrie, D. K.; First, P. N. *J. Am. Chem. Soc.* **1997**, *119*, 9279. (b) Chen, S.; Ingram, R. S.; Hostetler, M. J.; Pietron, J. J.; Murray, R. W.; Schaaff, T. G.; Khoury, J. T.; Alvarez, M. M.; Whetten, R. L. *Science* **1998**, *280*, 2098. (c) Chen, S.; Murray, R. W.; Feldberg, S. W. *J. Phys. Chem. B* **1998**, *102*, 9898.

(2) (a) Chen, S. *J. Am. Chem. Soc.* **2000**, *122*, 7420. (b) Chen, S.; Pei, R. *J. Am. Chem. Soc.* **2001**, *123*, 10607. (c) Chen, S.; Pei, R.; Zhao, T.; Dyer, D. J. *J. Phys. Chem. B* **2002**, *106*, 1903.

(3) (a) Chen, S.; Deng, F. *Proc. SPIE* **2002** (in press). (b) Chen, S. *J. Phys. Chem. B* **2000**, *104*, 663. (c) Chen, S.; Huang, K. *J. Cluster Sci.* **2000**, *11*, 405. (d) Zamborini, F. P.; Hicks, J. F.; Murray, R. W. *J. Am. Chem. Soc.* **2000**, *122*, 4515. (e) Chen, S.; Murray, R. W. *J. Phys. Chem. B* **1999**, *103*, 9996.

(4) (a) Peschel, S.; Schmid, G. *Angew. Chem., Int. Ed. Engl.* **1995**, *34*, 1442. (b) Freeman, R. G.; Grabar, K. C.; Allison, K. J.; Bright, R. M.; Davis, J. A.; Guthrie, A. P.; Hommer, M. B.; Jackson, M. A.; Smith, P. C.; Walter, D. G.; Natan, M. J. *Science* **1995**, *267*, 1629. (c) Andres, R. P.; Bein, T.; Dorogi, M.; Feng, S.; Henderson, J. I.; Kubiak, C. P.; Mahoney, W.; Osifchin, R. G.; Reinfenberger, R. *Science* **1996**, *272*, 1323. (d) Gittins, D. I.; Bethel, D.; Nichols, R. J.; Schiffrin, D. J. *J. Mater. Chem.* **2000**, *10*, 79. (e) Shipway, A. N.; Katz, E.; Wilner, I. *ChemPhysChem* **2000**, *1*, 18. (f) Mann, S.; Shenton, W.; Li, M.; Connolly, S.; Fitzmaurice, D. *Adv. Mater.* **2000**, *12*, 147. (g) Park, S.; Yang, P.; Corredor, P.; Weaver, M. J. *J. Am. Chem. Soc.* **2002**, *124*, 2428.

conventional molecular diode to those of a single-electron rectifier with increasing "softness" of electrolyte ions.

In this report, we describe a further study of this ion-induced rectifying quantized charging by incorporating a redox-active moiety into the chemical bridges that link the particles to the electrode surface and investigate the effect on the interfacial electron transfers involved. The electron-transfer chemistry of surface-immobilized viologen moieties is very sensitive to electrolyte ions, where the voltammetric peaks are very well-defined in solutions containing "hard" ions and diminish in the presence of "soft" ions. This is in great contrast to the case of nanoparticle quantized charging (*vide ante*). Thus, one can envision that by incorporating viologen moieties into the chemical linkages, rectification of interfacial electron-transfer can be achieved either at negative (viologen) or positive (nanoparticles) electrode potentials. In other words, by using these hybrid structures consisting of conventional and nanoscale redox-active entities, one can exploit their unique interactions with electrolyte ions to render the interfacial voltammetric responses similar to Coulomb blockade.

### Experimental Section

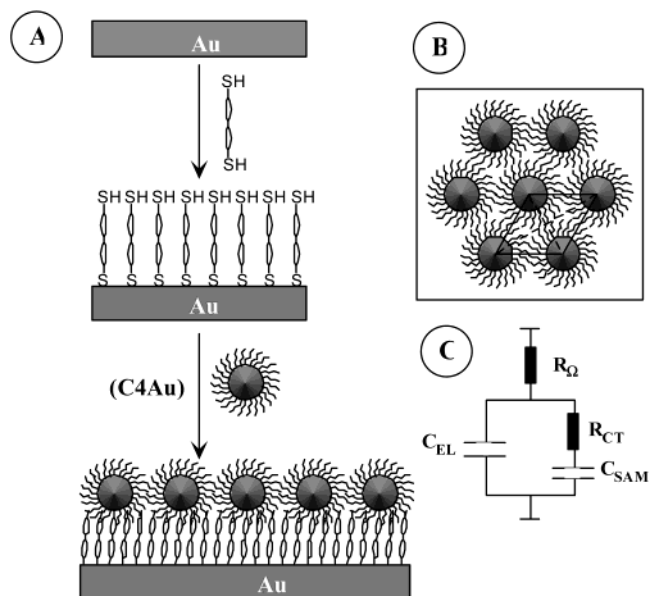
**Chemicals.** Ammonium hexafluorophosphate ( $\text{NH}_4\text{PF}_6$ , 99.5%, ACORS) was used as received. Ammonium nitrate ( $\text{NH}_4\text{NO}_3$ , Fisher) was recrystallized twice prior to use. All solvents were obtained from typical commercial sources and used as received as well. *N,N*-Bis(6-mercaptohexyl)-4,4'-bipyridinium dihexafluorophosphate (HSC6VC6SH) was synthesized, purified, and characterized according to a literature procedure.<sup>4d</sup> Water was supplied by a Barnstead Nanopure water system (18.3 M $\Omega$ ).

**Nanoparticles.** The synthesis and structural manipulations of monolayer-protected gold nanoparticles have been described previously.<sup>5</sup> Briefly, gold nanoparticles stabilized by a monolayer of *n*-butanethiolates (C4Au) were synthesized by the Schiffrin route.<sup>5a</sup> The particles were then fractionated by using a solvent and nonsolvent mixture (e.g., toluene and ethanol) to narrow the size dispersity and then underwent a thermal annealing process by refluxing in toluene for 4–8 h, resulting in mostly spherical shape and monodisperse size.<sup>6</sup> The final average particle core diameter was ca. 2.0 nm (determined by transmission electron microscopic measurements).

**Nanoparticle Assemblies.** The protocol for particles assembling onto a gold electrode surface is similar to that described earlier involving a two-step sequential anchoring mechanism (Scheme 1).<sup>3e</sup> First, a cleaned electrode was incubated into an acetonitrile solution of  $\alpha,\omega$ -dithiol viologen ligands (1 mM) for about 24 h. The electrode was then rinsed with copious acetonitrile and dried in a gentle nitrogen stream. This viologen-modified electrode was either used directly for electrochemical characterizations or immersed into a hexane solution of gold nanoparticles (1 mg/mL) for about 1 week to initiate particle surface anchoring. The time range was found to be sufficient for saturated coverage of nanoparticle assemblies though not yet optimized (longer immersion time did not result in appreciable difference of particle coverage). The electrode was then rinsed with copious hexane to remove loosely bound particles and again dried in a gentle nitrogen stream before being introduced into an electrochemical cell.

**Electrochemistry.** Electrochemical measurements were carried out with a BAS 100BW electrochemical workstation or CHI440 electrochemical quartz crystal microbalance (EQCM).

**Scheme 1. (A) Sequential Anchoring of Gold Nanoparticles to a Viologen Dithiol Self-Assembled Monolayers, (B) Hypothetical Hexagonal Distribution of Surface-Immobilized Nanoparticles, and (C) Randle's Equivalent Circuit<sup>a</sup>**



<sup>a</sup>  $R_{\Omega}$  is the solution (uncompensated) resistance,  $R_{CT}$  is the charge-transfer resistance, and  $C_{SAM}$  and  $C_{EL}$  are the interfacial capacitances from the collective contributions of all surface-anchored nanoparticles and the interparticle void space, respectively.<sup>2</sup>

Alternating current impedance spectra were acquired with an EG&G PARC 283 potentiostat coupled with an EG&G frequency response detector (Model 1025) within the frequency range of 1–10<sup>5</sup> Hz. Data analysis was done with a commercial software from EG&G. In typical electrochemical measurements, the gold electrode with viologen monolayers (and nanoparticle surface assemblies) was used as the working electrode, and Ag/AgCl (3 M NaCl, from BAS) and a Pt coil were used as the reference and counter electrodes, respectively. The solutions were deaerated for at least 20 min prior to data acquisition by water-saturated high-purity nitrogen and blanketed with an atmosphere of nitrogen during the entire experimental procedure.

For the EQCM measurements, the quartz crystals (International Crystal Manufacturing) were made from polished quartz plates with a resonant frequency of 8 MHz and the crystal diameter of 14 mm. A 10 nm layer of Cr was first deposited onto the center of the quartz crystals (dia. 5 mm) as the adhesion layer, followed by 100 nm of gold. The crystals were subjected to UV–ozone cleaning (UVO Cleaner Model 42, Jelight Co.) for 15 min prior to immersion into the viologen dithiol solution for monolayer coating. The frequency shift was measured in air as well as in solutions during in situ voltammetric measurements.

**FTIR Spectroscopy.** Reflection–absorption infrared studies of the surface assemblies were carried out with a Bruker Vector 33 FTIR spectrometer that was equipped with a Veemax surface accessory and a (LN<sub>2</sub>-cooled) MCT detector. Resolution was 4 cm<sup>-1</sup> and 800 scans were collected. The sample preparation was the same as described above for simple electrodes, except that a flat, thin gold film was used (gold films of 100 nm were deposited onto a microscope glass slide surface with a 10-nm Cr adhesion layer).

### Results and Discussion

In this section, we begin with a description of the voltammetric responses of viologen self-assembled monolayers, with emphases on the effects of electrolyte compositions on the faradaic reactions as well as charge-transfer kinetics. Fabrication and electrochemical studies

(5) (a) Brust, M.; Walker, M.; Bethel, D.; Schiffrin, D. J.; Whyman, R. *J. Chem. Soc., Chem. Comm.* **1994**, 801. (b) Whetten, R. L.; Shafiqullin, M. N.; Khoury, J. T.; Schaaff, T. G.; Vezmar, I.; Alvarez, M. M.; Wilkinson, A. *Acc. Chem. Res.* **1999**, *32*, 397. (c) Templeton, A. C.; Wuelfing, W. P.; Murray, R. W. *Acc. Chem. Res.* **2000**, *33*, 27. (d) Leff, D. V.; Ohara, P. C.; Heath, J. R.; Gelbart, W. M. *J. Phys. Chem.* **1995**, *99*, 7036.

(6) (a) Maye, M. M.; Zheng, W.; Leibowitz, F. L.; Ly, N. K.; Zhong, C.-J. *Langmuir* **2000**, *16*, 490. (b) Chen, S. *Langmuir* **2001**, *17*, 2878.

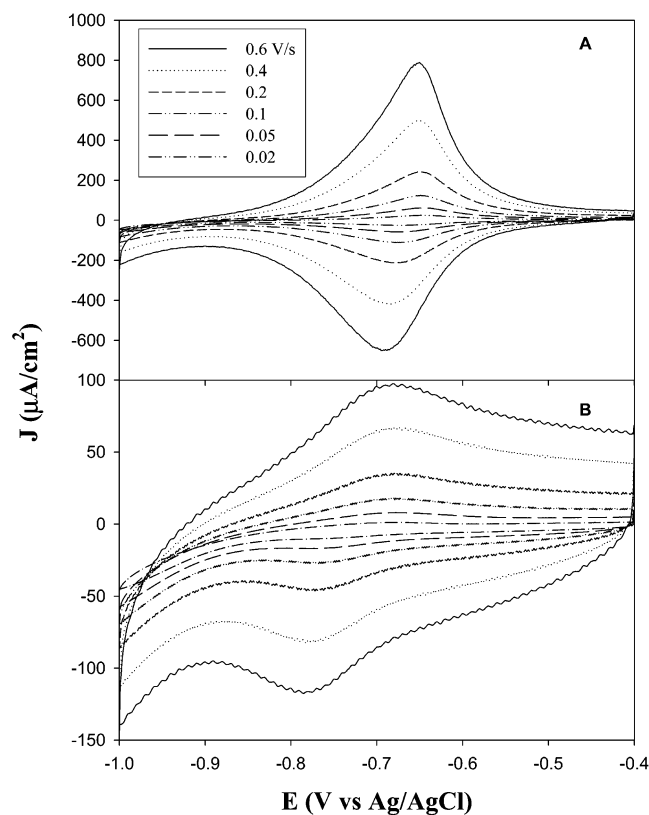


**Figure 1.** Cyclic voltammograms of HSC6VC6SH SAMs on a gold electrode surface in 0.10 M (A)  $\text{NH}_4\text{NO}_3$  and (B)  $\text{NH}_4\text{PF}_6$ . The electrode area is  $0.014 \text{ cm}^2$ . Potential scan rates are shown as figure legends.

of gold nanoparticle monolayers anchored by the  $\omega$ -thiol functional groups of the viologen surface layers will then follow. Ion-induced rectification of gold nanoparticle quantized capacitance charging will be examined in the context of the redox-active bipyridinium moieties. The opposite responses of the voltammetric currents of viologen functional groups and nanoparticle molecules to hydrophobic electrolyte ions will then be exploited to achieve rectification of interfacial charge transfer at controlled electrode potential positions, akin to Coulomb blockade.

**Viologen Self-Assembled Monolayers.** Figure 1 shows the cyclic voltammograms (CVs) of a self-assembled monolayer of viologen (HSC6VC6SH) on a gold electrode surface in 0.1 M  $\text{NH}_4\text{NO}_3$  (A) and  $\text{NH}_4\text{PF}_6$  (B) at various sweep rates. First, one can see that, in both solutions, there is a pair of rather well-defined voltammetric peaks with a formal potential at ca.  $-0.66$  and  $-0.73$  V, respectively. This is ascribed to the first  $1e^-$  reaction of the bipyridinium moieties involving a radical cation intermediate,  $\text{V}^{2+} + e \rightleftharpoons \text{V}^{\cdot+}$ . Also, the peak currents are both found to increase linearly with potential scan rates (not shown), consistent with surface-confined species. The effective surface coverage calculated from the respective slopes is, however, quite different,  $1.06 \times 10^{-9} \text{ mol/cm}^2$  in  $\text{NH}_4\text{NO}_3$  and  $2.77 \times 10^{-11} \text{ mol/cm}^2$  in  $\text{NH}_4\text{PF}_6$ . In addition, the peak spacing ( $\Delta E_p$ ) appears to be larger in  $\text{NH}_4\text{PF}_6$  than in  $\text{NH}_4\text{NO}_3$ ; for instance, at 0.1 V/s, the peak separation ( $\Delta E_p$ ) is 23 and 85 mV, respectively. This indicates that, while in these solutions the viologen electron-transfer (ET) reactions both behave (quasi)-reversibly, the ET kinetics appears to be impeded somewhat in the presence of  $\text{PF}_6^-$  (more details below). This might be interpreted on the basis of ion-pair formation between hydrophobic  $\text{PF}_6^-$  and the viologen moieties (vide infra). The ion-pairing can be manifested by the cathodic

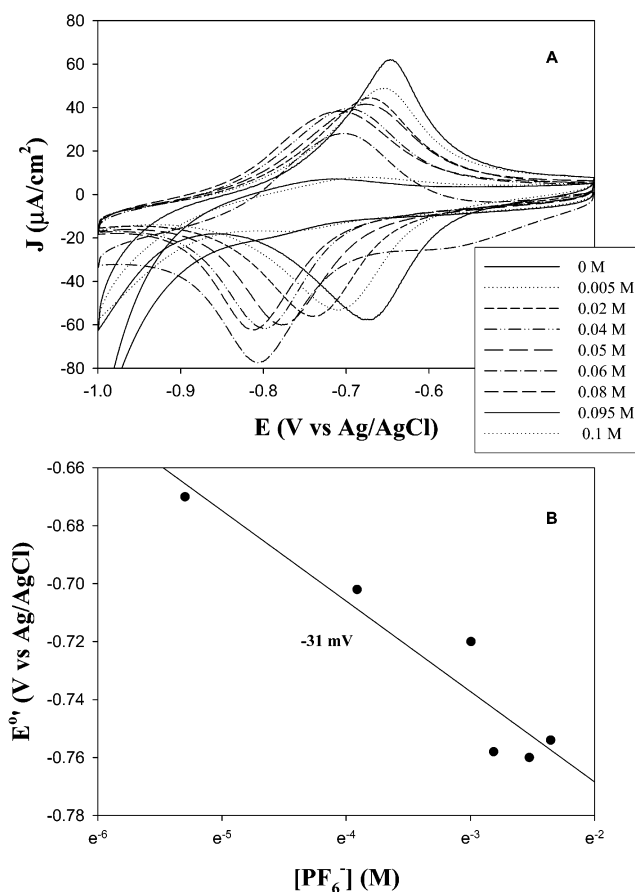


**Figure 2.** (A) Cyclic voltammograms of this same viologen monolayer in a solution containing  $\text{NH}_4\text{NO}_3$  and  $\text{NH}_4\text{PF}_6$ . The total electrolyte concentration is 0.10 M with varied amount of  $\text{NH}_4\text{PF}_6$  (shown as figure legends). Potential scan rate is 50 mV/s. (B) Variation of viologen formal potential with  $\text{KPF}_6$  concentration. Symbols are experimental data, and the line is a linear regression.

shift of the viologen formal potential ( $E_f$ ) with increasing  $\text{PF}_6^-$  concentration,<sup>7</sup>

$$E_f = E^{\circ'} + \frac{RT}{n_a F} \ln \frac{K_2}{K_1} - (p - q) \frac{RT}{n_a F} \ln [\text{PF}_6^-] \quad (1)$$

where  $E_f$  and  $E^{\circ'}$  are the formal potentials in the presence and absence of ion-binding, respectively;  $n_a$  is the (effective) number of electron transfer;  $K_2$  and  $K_1$  are the equilibrium constant with the monocationic and dicationic viologen functional groups, respectively;  $q$  and  $p$  are the number of anions bound to the reduced and oxidized forms of the viologen moieties, respectively; and others parameters have their usual significance. Figure 2A shows the CVs of the same viologen monolayer in an electrolyte solution with varied concentrations of  $\text{NH}_4\text{PF}_6$  (with  $\text{NH}_4\text{NO}_3$  to maintain the total concentration at 0.10 M). One can see that with increasing  $\text{PF}_6^-$  concentration, the voltammetric profile shifts cathodically, and the formal potential indeed exhibits a linear relationship with  $\ln[\text{PF}_6^-]$  (Figure 2B), as dictated by eq 1. The slope of  $-31$  mV is only slightly greater than  $-25$  mV, as anticipated for a 1:1 binding ratio between viologen moieties and  $\text{PF}_6^-$  ions, as observed previously.<sup>7</sup> From the intercept, one can also evaluate the

(7) (a) Sagara, T.; Maeda, H.; Yuan, Y.; Nakashima, N. *Langmuir* **1999**, *15*, 3823. (b) Hiley, S. L.; Buttry, D. A. *Colloid Surf. A: Physicochem. Eng. Aspects* **1994**, *84*, 129. (c) Mortimer, R. J.; Anson, F. C. *J. Electroanal. Chem.* **1982**, *138*, 325.

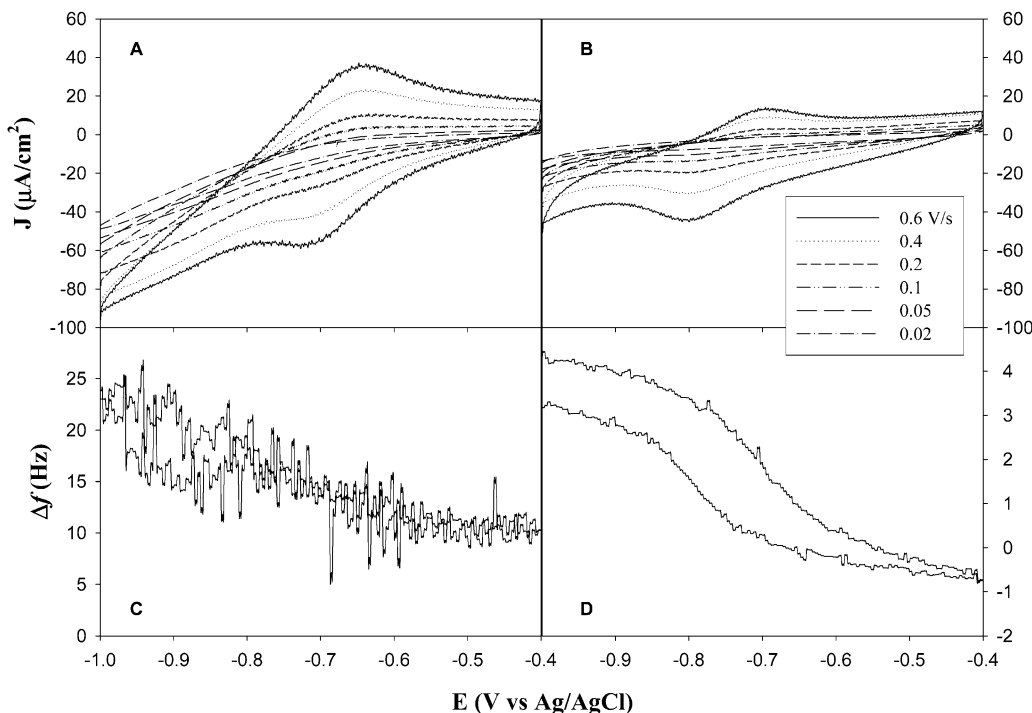


**Figure 3.** Cyclic voltammograms and frequency change of a HSC6VC6SH monolayer on a quartz crystal electrode surface in 0.1 M (A)  $\text{NH}_4\text{NO}_3$  and (B)  $\text{NH}_4\text{PF}_6$ . Potential scan rates are shown in figure legends. Panels C and D show the corresponding frequency changes with electrode potentials. The potential scan rate is 20 mV/s.

**Table 1. Number of Water Molecules Lost from the Interface Concurrent with the Desorption of  $\text{PF}_6^-$  Ions in the Reduction of the Bipyridinium Moieties**

$[\text{NH}_4\text{PF}_6]$ (M) <sup>a</sup>	0.005	0.02	0.04	0.05	0.06	0.08	0.095	0.10
no. of $\text{H}_2\text{O}$	1.3	1.7	2.0	1.7	3.1	3.2	3.6	4.9

<sup>a</sup> With  $\text{NH}_4\text{NO}_3$  to maintain the solution ionic strength at 0.1 M.

ratio of the binding constants of  $\text{PF}_6^-$  ions to the oxidized and reduced forms of viologen,  $K_1/K_2 = 6.78 \times 10^2 \text{ M}^{-1}$  (using  $E^\circ = -0.66 \text{ V}$  and  $n_a = 1$ ). Using a binary mixture of KF and  $\text{KPF}_6$  (total concentration 0.4 M), Sagara et al.<sup>7a</sup> estimated  $K_1/K_2$  to be  $1.2 \times 10^4 \text{ M}^{-1}$  for a self-assembled monolayer of *N*-butyl-*N'*-(4-mercaptobutyl)-4,4'-bipyridinium on a gold electrode surface. Despite this discrepancy, both studies indicate that the binding of  $\text{PF}_6^-$  ions to dicationic viologen ( $\text{V}^{2+}$ ) is much stronger than that to the radical monocation ( $\text{V}^{\cdot+}$ ).

Electrochemical quartz crystal microbalance (EQCM) studies provide additional experimental insight into the ion-pairing mechanism. Figure 3 shows the cyclic voltammograms of a HSC6VC6SH self-assembled monolayer in 0.1 M  $\text{NH}_4\text{NO}_3$  (A) and  $\text{NH}_4\text{PF}_6$  (B) at various sweep rates. The responses are similar to those observed in Figure 1. Figure 3C,D depicts the corresponding frequency changes ( $\Delta f$ ) with potential scans. The frequency change ( $\Delta f$ ) directly reflects the interfacial mass change ( $\Delta m$ , per unit surface area), according to the Sauerbrey equation<sup>8</sup>

$$\Delta m = -\frac{\sqrt{\rho_q \mu_q} \Delta f}{2f_0^2} \quad (2)$$

where  $f_0$  is the resonant frequency of the quartz crystal (8 MHz in the present case),  $\rho_q$  is the density of quartz (2.648 g/cm<sup>3</sup>), and  $\mu_q$  is its shear modulus ( $2.947 \times 10^{11}$  dyn/cm<sup>2</sup> for AT-cut quartz). One can see that in both solutions, the frequency increases upon the reduction of

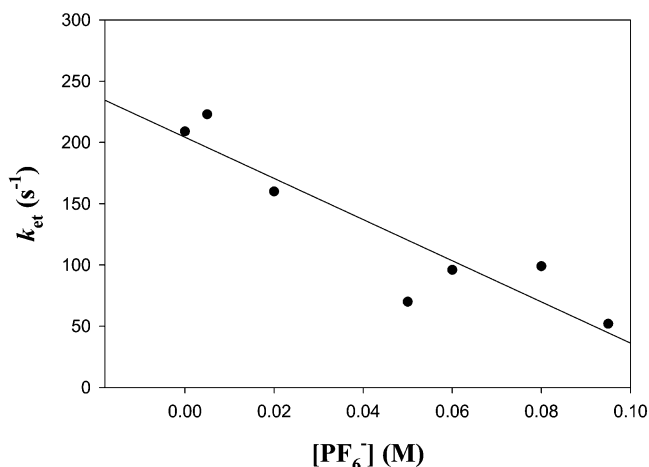


**Figure 4.** Variation of the electron-transfer rate constant of the viologen moiety with  $\text{NH}_4\text{PF}_6$  concentrations. The line is for eye-guiding only.

dicationic viologen moieties into monovalent radical cation intermediates, which is attributable to the release of counteranions from the interfacial viologen charge centers (and hence mass decrease). The frequency increase in  $\text{NH}_4\text{NO}_3$  is about 13 Hz, while that for  $\text{NH}_4\text{PF}_6$  is only 4 Hz, indicating that the adsorption and release of  $\text{NO}_3^-$  ions are more facile than those of  $\text{PF}_6^-$  ions. This is associated with the stronger interactions between the viologen moieties and the hydrophobic  $\text{PF}_6^-$  ions and hence the more compact monolayer structure. From the frequency change, one can also estimate the number of solvent molecules ( $\text{H}_2\text{O}$ ) lost during this reduction process, as listed in Table 1. It can be seen that with increasing  $\text{PF}_6^-$  concentration, the number of  $\text{H}_2\text{O}$  lost from the interface is also increasing, e.g., from 1.3 at 5 mM to 4.9 at 0.1 M. This is slightly smaller than previous literature results, where it was found that ca. five water molecules per  $\text{PF}_6^-$

(8) Sauerbrey, G. Z. Z. Phys. Chem. 1959, 155, 206.

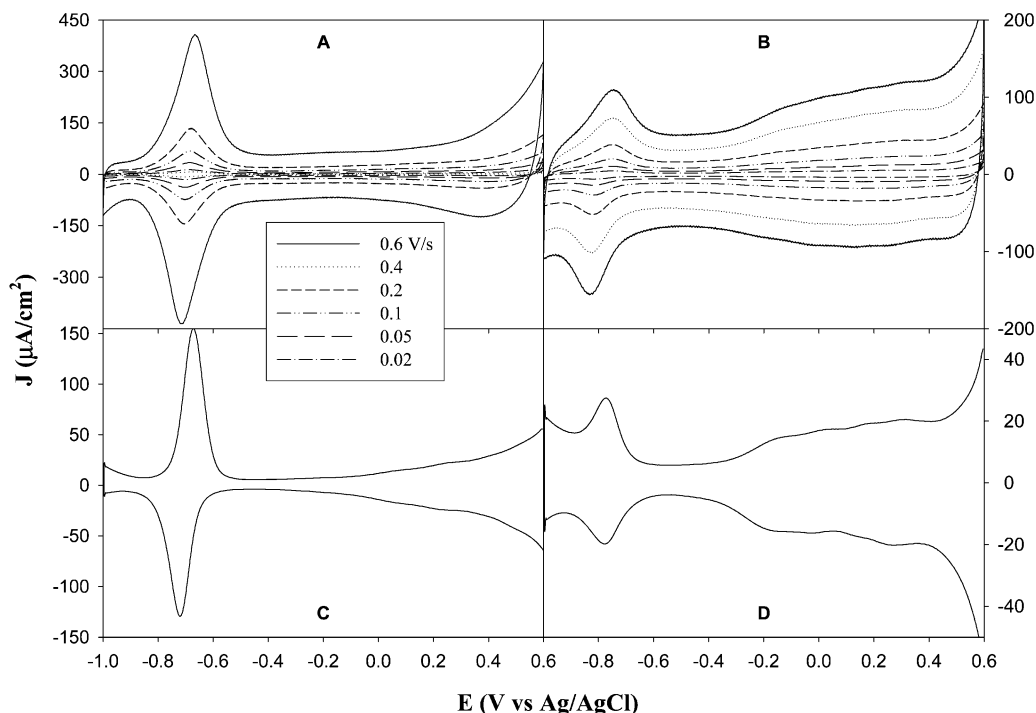


**Figure 5.** Cyclic voltammograms of C4Au nanoparticles assembled onto the viologen monolayers (Figure 1) in a solution of (A) 0.1 M  $\text{NH}_4\text{NO}_3$  and (B) 0.005 M  $\text{NH}_4\text{NO}_3$  and 0.095 M  $\text{NH}_4\text{PF}_6$ . Potential scan rates are shown in figure legends. Panels C and D are the corresponding differential pulse voltammograms (DPVs). Pulse amplitude is 50 mV, and DC ramp is 10 mV/s.

ion were lost during the reduction of the bipyridinium moieties.<sup>9</sup>

Additionally, one can see from Figures 2 and 3 that the viologen voltammetric peak currents diminish with increasing  $\text{PF}_6^-$  concentration. In solutions containing only 0.1 M  $\text{NH}_4\text{PF}_6$ , the viologen voltammetric currents are almost 1 order of magnitude smaller. This might be ascribed to the effects of ion-pairing on viologen interfacial charge transfer, as it has been observed previously that ion-pairing with  $\text{PF}_6^-$  ions renders the viologen moieties electrochemically inactive.<sup>7c</sup> It appears that the binding of negatively charge  $\text{PF}_6^-$  ions to the cationic viologen moieties creates additional energetic barrier for electroreduction of the viologen moieties and thus hinders the faradaic reactions. Figure 4 shows the effect of  $\text{PF}_6^-$  concentration on viologen charge-transfer kinetics, where the rate constants ( $k_{\text{et}}$ ) were evaluated from ac impedance measurements<sup>2,10</sup>

$$k_{\text{et}} = \frac{1}{2R_{\text{CT}}C_{\text{SAM}}} \quad (3)$$

where  $R_{\text{CT}}$  is the charge-transfer resistance and  $C_{\text{SAM}}$  is the collective (pseudo)capacitance of surface-immobilized viologen moieties (Scheme 1C). One can see that in this particular system with a hexyl spacer, the rate constant is on the order of  $10\text{--}100\text{ s}^{-1}$  and decreases with increasing concentration of  $\text{PF}_6^-$  ions, e.g., from  $210\text{ s}^{-1}$  at 0 M (i.e., in 0.1 M  $\text{NH}_4\text{NO}_3$ ) to  $52\text{ s}^{-1}$  at 0.095 M (plus 0.005 M  $\text{NH}_4\text{NO}_3$ ; the ACV signal in 0.1 M  $\text{NH}_4\text{PF}_6$  is too low for a meaningful evaluation). In comparison, previously, using the electroreflectance method, Sagara et al.<sup>7a</sup> estimated the  $k_{\text{et}}$  of an N-pentyl-N-(5-mercaptopentyl)-4,4'-bipyridinium monolayer to be on the order of  $10^4\text{ s}^{-1}$  in 0.1 M  $\text{Na}_2\text{SO}_4$ .

It should be noted that in earlier studies of ion-induced rectification of gold nanoparticle quantized capacitance charging in aqueous solutions,<sup>2</sup> the corresponding electron-transfer kinetics was found to be a few orders of magnitude smaller than that evaluated with nanoparticle dropcast thick films.<sup>11,12</sup> It is likely that the discrepancy observed there might also arise from the binding of hydrophobic anions to the particle molecules, akin to the present case with viologen moieties. These studies demonstrate that simple ion chemistry might be exploited to manipulate the interfacial charge transfer (more details below).

**Nanoparticle Surface Organized Assemblies.** Dithiol linkers have been used previously to anchor gold nanoparticles onto electrode surfaces by taking advantage of place-exchange reactions.<sup>2,3</sup> The resulting gold particle surface assemblies are found to exhibit quantized charging characters.<sup>2,3</sup> In particular, in aqueous solutions containing hydrophobic electrolyte ions, the quantized charging features can be rectified by the ion-pair formation between nanoparticle molecules and hydrophobic ions.<sup>2</sup> This is interpreted on the basis of manipulation of electrode interfacial capacitance by ion-pairing chemistry (Randle's equivalent circuit, Scheme 1C).<sup>2</sup> In the present work, the fabrication of gold nanoparticle monolayers is achieved by the sequential anchoring route depicted in Scheme 1. Here a monolayer of C4Au particles was constructed by incubating the electrode with a preformed HSC6VC6SH adlayer into a C4Au particle solution in hexane for 7–10 days. The total frequency decrease measured in air is 281 Hz (relative to that with only the viologen monolayer), as

(11) (a) Evans, S. D.; Johnson, S. R.; Cheng, Y. L.; Shen, T. *J. Mater. Chem.* **2000**, *10*, 183. (b) Doty, R. C.; Yu, H.; Shih, C. K.; Korgel, B. A. *J. Phys. Chem. B* **2001**, *105*, 8291. (c) Snow, A. W.; Wohltjen, H. *Chem. Mater.* **1998**, *10*, 947. (d) Clarke, L.; Wybourne, M. N.; Brown, L. O.; Hutchison, J. E.; Yan, M.; Cai, S. X.; Keana, J. F. W. *Semicond. Sci. Technol.* **1998**, *13*, A111.

(12) (a) Wuelfing, W. P.; Green, S. J.; Pietron, J. J.; Cliffl, D. E.; Murray, R. W. *J. Am. Chem. Soc.* **2000**, *122*, 11465. (b) Hicks, J. F.; Zamborini, F. P.; Osisek, A. J.; Murray, R. W. *J. Am. Chem. Soc.* **2001**, *123*, 7048.

(9) John, S. A.; Kitamura, F.; Nanbo, N.; Tokuda, K.; Ohsaka, T. *Langmuir* **1999**, *15*, 3816.

(10) Creager, S. E.; Wooster, T. T. *Anal. Chem.* **1998**, *70*, 4257.

evaluated by EQCM measurements, corresponding to a final coverage of gold particles of about  $2.78 \times 10^{-11}$  mol/cm<sup>2</sup>. By assuming a hexagonal (close-packed) distribution of the surface-immobilized nanoparticles (Scheme 1B), the center-to-center interparticle distance is estimated to be 2.83 nm. Considering that the physical diameter of a particle molecule is approximately 3.02 nm (particle core diameter of 2 nm plus two chain lengths of the fully extended butanethiolate ligands, 0.51 nm each as calculated by Hyperchem), this indicates some degree of ligand intercalation between the protecting shells of neighboring particles. Thus, it can be deemed as full-monolayer coverage. Figure 5 shows the corresponding voltammetric responses in 0.1 M NH<sub>4</sub>NO<sub>3</sub> (A) and NH<sub>4</sub>PF<sub>6</sub> (B) at various sweep rates. The corresponding differential pulse voltammograms are shown in panels C and D, respectively. First, it can be seen that, again, the viologen voltammetric currents are much larger in NH<sub>4</sub>NO<sub>3</sub> than in NH<sub>4</sub>PF<sub>6</sub>, as observed above. Second, in the presence of PF<sub>6</sub><sup>-</sup> ions, the discrete charging characteristics of gold nanoparticles are very well-defined (panel D), in comparison to the case in NH<sub>4</sub>NO<sub>3</sub>, where only featureless responses are found (panel C), as observed earlier.<sup>2</sup> From the potential spacing ( $\Delta V$ ) between neighboring charging peaks, one can evaluate the nanoparticle effective molecular capacitance ( $C_{MPC}$ ) to be ca. 1.06 aF, similar to that obtained with nanoparticle monolayers anchored by alkanedithiols.<sup>2</sup> It should be noted that the quantized charging features are only observed at positive electrode potentials, a behavior interpreted by the ion-induced rectification of nanoscale electron transfer.<sup>2</sup>

Previously, using alkanedithiol chemical linkers to fabricate nanoparticle surface organized assemblies,<sup>2</sup> the ion-pairing between hydrophobic electrolyte ions and nanoparticle molecules was found to be also consistent with eq 1 with a 1:1 ratio between the number of anions bound to the particles and particle charge states.<sup>2</sup> Figure 6A depicts the effects of PF<sub>6</sub><sup>-</sup> concentration on the voltammetric responses of gold nanoparticle monolayers with viologen dithiol linkers. It can be seen that overall the voltammetric profiles shift cathodically with increasing PF<sub>6</sub><sup>-</sup> concentration, again as dictated by eq 1. More importantly, one can see that at low concentrations of PF<sub>6</sub><sup>-</sup> ions, the voltammetric current at negative potentials is much larger than that in the positive potential regime, because of the faradaic reactions of the viologen moieties, whereas, with increasing concentration of PF<sub>6</sub><sup>-</sup> ions, the viologen redox peaks diminish and concurrently the nanoparticle quantized charging currents start to grow and become more comparable to the viologen redox currents. One can therefore envision that by taking advantage of the unique interactions between hydrophobic electrolyte ions and (conventional) redox-active moieties as well as particle molecules, one can rectify the nanoscale electron transfer at a controlled potential position.

With regard to the potential shift with PF<sub>6</sub><sup>-</sup> concentration, it can be seen from Figure 6B that for the viologen moieties, the slope is -22 mV (●), which is somewhat smaller than that (-31 mV) observed above without the particle overlayer (Figure 2). One plausible scenario is that the adsorption of particle molecules onto the viologen monolayers leads to ligand intercalation between the particle protecting shell and the neighboring viologen chains, pushing the overall monolayer to be somewhat more compact and consequently hindering the release and capture of PF<sub>6</sub><sup>-</sup> ions by the bipyridinium moieties. For the nanoparticles at varied charge states, the slopes are generally close to -25 mV as expected for a 1:1 ratio between the number of particle-bound PF<sub>6</sub><sup>-</sup> ions and the

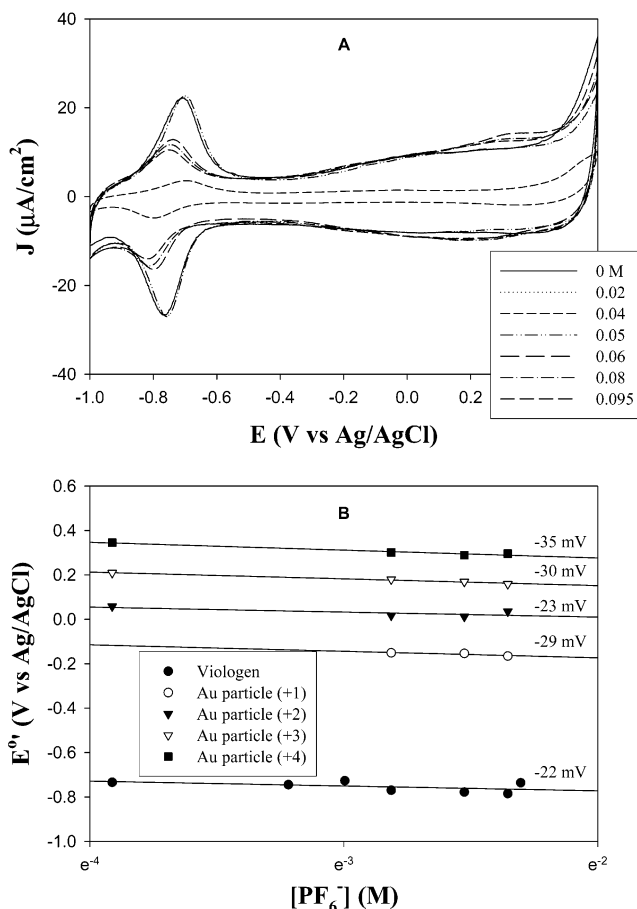


**Figure 6.** (A) Cyclic voltammograms of C4Au nanoparticles assembled onto the viologen monolayers (Figure 5) in a solution of  $(0.1 - x)$  M NH<sub>4</sub>NO<sub>3</sub> and (B)  $x$  M NH<sub>4</sub>PF<sub>6</sub>. Potential scan rate is 50 mV/s. (B) Variation of formal potentials of viologen moieties and nanoparticle quantized charging with NH<sub>4</sub>PF<sub>6</sub> concentrations. Symbols are experimental data, and lines are linear regressions; the slope of each is shown in the figure.

particle charge state, e.g., -29 mV at  $z = +1$  (○), -23 mV at  $z = +2$  (▼), -30 mV at  $z = +3$  (▽), and -35 mV at  $z = +4$  (■). The results are quite consistent with earlier data where particles monolayers were linked by alkanedithiols.<sup>2</sup>

**Electrode Double-Layer Capacitance.** It should be noted that the binding of PF<sub>6</sub><sup>-</sup> ions to the interfacial layers has rather substantial effects on electrode double-layer capacitance ( $C_{DL}$ ). Figure 7 shows the variation of  $C_{DL}$  measured at -0.45 V with PF<sub>6</sub><sup>-</sup> concentration. First, one can see that for viologen monolayers, the double-layer capacitance exhibits a slight increase with increasing PF<sub>6</sub><sup>-</sup> concentration, and a small stepwise incremental transition appears to occur at 0.04 M. This might again be ascribed to the ion-pair formation between the PF<sub>6</sub><sup>-</sup> ions and the bipyridinium moieties as well as partition of PF<sub>6</sub><sup>-</sup> ions into the viologen monolayers. Second, in general, the adsorption of a gold nanoparticle overlayer increases the electrode double-layer capacitance, most probably because the presence of nanosized gold cores increases the effective interfacial dielectric. However, in the presence of a gold nanoparticle overlayer, the effects are more complicated. It appears that initially  $C_{DL}$  is virtually invariant at low PF<sub>6</sub><sup>-</sup> concentrations ( $\leq 0.02$  M), with an abrupt dip at 0.04 M, then remains almost unchanged within the concentration range of 0.05–0.08 M, and increases rather rapidly at higher concentrations ( $\geq 0.08$  M).

While the details remain unclear at the moment, these concentration effects might again arise from the specific

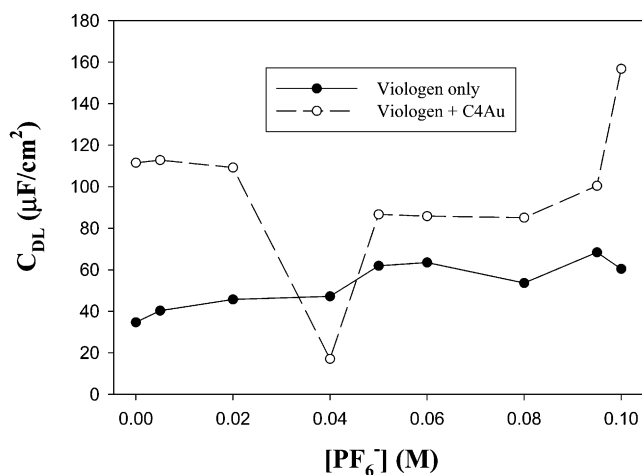


**Figure 7.** Variation of electrode double-layer capacitance ( $C_{DL}$ ) with  $\text{NH}_4\text{PF}_6$  concentration in the presence and absence of the C4Au particle adsorbed monolayers.  $C_{DL}$  is evaluated by the interfacial charging currents at varied potential scan rates at ca.  $-0.45$  V. Symbols are experimental data, and lines are for eye-guiding only.

interactions between  $\text{PF}_6^-$  ions and the viologen moieties embedded in the monolayer (adsorption to the surface-supported particle molecules is expected to be minimal as at  $E = -0.45$  V, their ion-pair formation is not favored<sup>2</sup>). It should be noted that adsorption of the gold nanoparticle overlayer renders the surface assemblies more ordered, partly because of ligand intercalation between the alkanethiolate protecting shell and the viologen ligands. This was evidenced by surface reflection-absorption FTIR measurements, where the symmetric ( $d^+$ ) and antisymmetric ( $d^-$ )  $\text{CH}_2$  stretching vibrations were found to red-shift somewhat (see the Supporting Information for the spectra).<sup>13</sup> The sudden decrease of  $C_{DL}$  at  $[\text{PF}_6^-] = 0.04$  M observed above (Figures 6 and 7) suggests that at this concentration, there might be substantial surface rear-

rangements of the viologen monolayers induced by the penetration of  $\text{PF}_6^-$  ions into the monolayer interior, leading to more compact surface structures. Further increase of  $\text{PF}_6^-$  concentrations in solutions results in enhanced partition of  $\text{PF}_6^-$  into the surface monolayers and hence increase in double-layer capacitance.

### Concluding Remarks

Gold nanoparticle surface assemblies were fabricated by using dithiol derivatives of viologen. The charge-transfer chemistry of both the bipyridinium moieties and the nanoparticle molecules was found to be sensitive to the nature of electrolyte ions. In the presence of hydrophobic anions ( $\text{PF}_6^-$ ), it was found that the faradaic reactions of the viologen functional groups was impeded, whereas the rectifying quantized charging currents of nanoparticle molecules were facilitated at increasing  $\text{PF}_6^-$  concentrations. Since the formal potential of viologen charge-transfer is far more negative than the onset potential for nanoparticle rectified quantized charging, one can envision that by using a hybrid structure involving conventional redox-active moieties and nanoscale particle entities, the interfacial charge-transfer can be manipulated at a controlled electrode potential. The resulting overall voltammetric responses become analogous to those of a semiconductor molecular diode.

**Acknowledgment.** The authors are grateful to Ms. Junge Lu for the assistance in the synthesis of the viologen ligands. This work was supported by the National Science Foundation (CAREER Award CHE-0092760), the ACS Petroleum Research Fund, and the SIU Materials Technology Center. S.C. is a Cottrell Scholar of Research Corporation.

**Supporting Information Available:** FTIR spectra of viologen derivatives (HSC6VC6SH) in a KBr pellet, HSC6VC6SH self-assembled monolayers on a gold surface, and HSC6VC6SH self-assembled monolayers with an overlayer of gold nanoparticles (C6Au). This material is available free of charge via the Internet at <http://pubs.acs.org>.

LA025966Y

(13) (a) Dubois, L. H.; Nuzzo, R. G. *Annu. Rev. Phys. Chem.* **1992**, *43*, 437. (b) Bain, C. D.; Whitesides, G. M. *Angew. Chem., Int. Ed. Engl.* **1989**, *28*, 506.